JOURNAL OF THERMOPHYSICS AND HEAT TRANSFER
Vol. 20, No. 3, July–September 2006

Flight Extrapolation of Plasma Wind Tunnel Stagnation Region Flowfield

P. F. Barbante*
Politecnico di Milano, Milano 20133, Italy
and
O. Chazot†
Von Karman Institute for Fluid Dynamics, Rhode St. Genèse 1640, Belgium

Development of reusable space vehicles requires a precise qualification of their thermal protection system materials. The catalytic properties are usually determined in plasma wind tunnels for test conditions relevant to the flight mission program. Therefore, for such a situation, it is important to have a methodology that allows the correct extrapolation of the ground test conditions to the real flight ones and vice-versa. The local heat transfer simulation concept presented in this paper is a possible strategy for accomplishing this task. Computational results show that the ground test conditions are indeed correctly extrapolated to the flight ones and a simple method of accounting for possible discrepancies between the two configurations is presented.

Nomenclature

$\mathcal{D}_{ij}$	=	binary diffusion coefficient between species i and j, m^2/s
F	=	u/u_e, nondimensional tangential velocity
g	=	h/h_e, nondimensional mixture enthalpy
H	=	mixture total enthalpy, J/kg
h	=	mixture enthalpy, J/kg
h_i	=	enthalpy of species i, J/kg
Le	=	Lewis number
J_i	=	nondimensional mass diffusion flux of species i
l_0	=	$\rho\mu/\rho_e\mu_e$, Chapman–Rubesin parameter
N_s	=	number of species in the mixture
Pr	=	Prandtl number
p	=	pressure, Pa
Q	=	normalized heat flux
q	=	heat flux, W/m^2
R	=	body nose radius, m
T	=	mixture temperature, K
u, v	=	tangential and normal velocity components, m/s
V	=	velocity, m/s
$\tilde{V}$	=	nondimensional transformed normal velocity
$\dot{w}_i$	=	nondimensional mass production rate of species i
x, y	=	Cartesian coordinates, m
y_i	=	mass fraction of species i
β	=	$\partial u/\partial x$, velocity gradient, s^{-1}
γ	=	wall catalytic recombination probability
$\hat{\eta}$	=	transformed y coordinate
λ	=	mixture thermal conductivity, W/(m K)
μ	=	mixture viscosity, m^2/s
ρ	=	mixture density, kg/m^3

Subscripts

e	=	boundary layer outer edge
w	=	wall surface
∞	=	free stream

Superscripts

f	=	flight
FC	=	fully catalytic
NC	=	noncatalytic
t	=	ground facility

Received 15 April 2005; revision received 21 June 2005; accepted for publication 22 June 2005.

*Researcher, Dipartimento di Matematica, Piazza Leonardo da Vinci 32; barbante@mate.polimi.it.

†Assistant Professor, Aeronautics and Aerospace Department, Ch. de Waterloo 72; chazot@vki.ac.be.

Introduction

DESIGN and testing of thermal protection system (TPS) materials, which are used to protect space vehicles from heat load during the (re-)entry phase, are a major issue for the definition of space missions.[1,2] The determination of the catalytic properties of TPS materials is especially crucial for the design of an optimal flight strategy. As a matter of fact the stagnation region heat flux for a fully catalytic wall can be more than twice the heat flux for a noncatalytic one.[3] Such situation requires ground facilities able to provide representative testing conditions for the evaluation of the material performances. TPS materials should be tested in real flight conditions make it possible to rely safely on their catalytic properties. However, it is known that the complete real flight conditions cannot be exactly duplicated in a ground test facility.[4] The usual strategy for overcoming this problem is to resort to some kind of partial simulation: only some characteristics of the flight environment, that are of interest in the specific experiment, are reproduced.[5]

Plasma wind tunnels, which can provide dissociated flows for large characteristic times, have been widely exploited, in particular for stagnation point testing configuration. On one hand, supersonic arc-jet wind tunnels have been used to determine TPS catalytic properties[6]; on the other hand, subsonic plasma wind tunnels, known as Plasmatron facilities, have also been demonstrated to be suitable for TPS catalyticity studies.[7] The testing methodology in subsonic plasma flows has been implemented for the high-enthalpy facilities at the von Karman Institute (VKI). This approach of catalycity determination makes use of dedicated experimental procedures, combined with accurate computational fluid dynamics computations of the flowfield inside the ground facility.[8–10]

In this paper we want to start from experimental test results pertinent to this VKI methodology and to extrapolate them up to the corresponding real flight application. The results make it possible as well to verify the hypothesis of the flight extrapolation method and to discuss detailed features of hypersonic flows.

Local Heat Transfer Simulation Concept

One of the most critical parts of a (re-)entry vehicle is the stagnation point region, which is often subject to the highest heat flux. It is therefore important that the testing conditions in the ground facility

correctly reproduce at least the real flight environment around the stagnation point of the aerospace vehicle. The other way around, one has also to be able to correctly determine to which flight conditions the ground test conditions correspond. The extrapolation from the ground test conditions to the real flight conditions is done by means of the local heat transfer simulation (LHTS) technique.[11] Here by flight conditions we mean a set of freestream conditions, such as pressure, temperature, and Mach number, that will reproduce, in the boundary layer near the stagnation point of the space vehicle, the same kind of environment found in the ground facility.

We start by considering the Fay and Riddell[12] and Goulard[13] formulae for the heat flux at the stagnation point of a body immersed in a reacting flow. The Fay and Riddell formula is

$$q_w = 0.76 Pr^{-0.6} (\rho_e \mu_e)^{0.4} (\rho_w \mu_w)^{0.1} \beta_e^{0.5} (H_e - h_w) \left[1 + (Le^{\alpha} - 1)(h_{D,e}/H_e)\right] \quad (1)$$

$h_{D,e}$ is the dissociation enthalpy, which is equal to

$$\sum_{i=1}^{N_s} y_{i,e} \Delta h^0_{F,i}$$

($\Delta h^0_{F,i}$ is the enthalpy of formation of species i and $y_{i,e}$ its mass fraction). The exponent α is equal to 0.52 for an equilibrium boundary layer and to 0.63 for a frozen boundary layer with fully catalytic wall. β_e is the velocity gradient at the boundary layer outer edge. The Goulard formula is valid for a frozen boundary layer with an arbitrarily catalytic wall and it is equal to

$$q_w = 0.664 Pr^{-\frac{2}{3}} (\beta_e \rho_e \mu_e)^{0.5} H_e \left[1 + \left(Le^{\frac{2}{3}} \phi - 1\right)(h_{D,e} y_e / H_e)\right] \quad (2)$$

where y_e is the atom mass fraction at the boundary layer edge and ϕ is a factor that takes into account the wall catalyticity.

The two formulae are very similar and they state that the stagnation point heat flux is a function of the velocity gradient, flow enthalpy, density, and chemical composition (which appears in the determination of the dissociation enthalpy $h_{D,e}$) at the boundary layer outer edge and of the wall enthalpy and catalyticity. To have a correct simulation, the wall conditions should be the same in flight and in the wind tunnel. It follows that the heat flux is equal in the two cases if the outer edge enthalpy, chemical composition, density, or pressure and velocity gradient are the same for wind tunnel and flight. If we make the somewhat restrictive assumption that the flow is near equilibrium at the stagnation point, it follows that the heat flux is the same in flight and in the wind tunnel if the total enthalpy (H_e), the pressure (p_e), and the velocity gradient (β_e) at the outer edge of the boundary layer are the same:

$$H_e^f = H_e^t \qquad p_e^f = p_e^t \qquad \beta_e^f = \beta_e^t \quad (3)$$

The next point is to determine the freestream flight conditions and the flying body geometry that will ensure the needed values of H_e, p_e, and β_e in the stagnation region. This task is accomplished by means of the formulae

$$h_\infty^f + \tfrac{1}{2} V_\infty^{f2} = H_e^t \quad (4)$$

$$p_\infty^f + \rho_\infty^f V_\infty^{f2} = p_e^t \quad (5)$$

$$\sqrt{\left(\tfrac{8}{3}\right)\left(\rho_\infty^f / \rho_e^f\right)}\left(V_\infty^f / R_\infty^f\right) = \beta_e^t \quad (6)$$

Equations (4) and (5) are the conservation of energy and momentum for the monodimensional flow on the stagnation line respectively; Eq. (6) is an expression for the velocity gradient computed from the thin shock layer theory[14] (where R_∞^f is the nose radius of the flying body). Although these three equations are only an approximate description of the phenomena that are really happening on the stagnation line, they are still accurate enough for the determination of the flight conditions. Equation (4) can be simplified by taking into account that, at hypersonic flight speed, $h_\infty^f \ll \frac{1}{2} V_\infty^{f2}$; similarly, Eq. (5) is simplified by means of the inequality $p_\infty^f \ll \rho_\infty^f V_\infty^{f2}$. With these simplifications Eq. (4) gives the flight speed, Eq. (5) the freestream density and therefore the altitude, and Eq. (6) the flying body nose radius, all the other quantities being known.

For the assessment of the LHTS concept two series of computations are performed for different levels of wall catalycity. Boundary layer outer edge flow conditions are taken from VKI plasma wind tunnel experiments. The first series of computations characterizes the flowfield at the stagnation point of the TPS sample; the second series of computations defines the corresponding real flight situation. Details on the numerical approach are given in the next section.

Governing Equations and Numerical Methods

We make the following main assumptions: the flow is laminar and axisymmetric; the influence of body forces due to external fields is neglected; the fluid is made out of N_S chemical species, each a thermally perfect gas. Transport coefficients (viscosity μ, thermal conductivity λ, binary diffusion coefficients $\mathcal{D}_{ij}$) are computed with the Chapman–Enskog method.[15] Thermodynamic properties are computed by means of statistical mechanics[15]; in the calculations shown here, the rigid rotator, harmonic oscillator model is chosen for the molecular species. Diffusion fluxes are computed by means of the exact Stefan–Maxwell equations[16,17] instead of the simplified and inconsistent Fick's law often found in literature. This choice is important if one wants to correctly compute the heat flux[16,17] and it is therefore mandatory for the correctness of the LHTS technique. The chemical forward reaction rates are computed from Arrhenius data fits given in Ref. 18; the backward reaction rates are computed from the forward ones and the equilibrium constant, the latter being computed from statistical mechanics.[15] Wall chemical reactions are taken into account by means of a wall catalyticity model that allows a correct reproduction of the TPS material properties.[16,19]

The first series of computations is performed in the stagnation region of the TPS material sample; a boundary layer code developed by the first author is used.[19] Such a choice is justified by the fact that boundary layer equations are perfectly equivalent to Navier–Stokes ones at the stagnation point.[20] For the sake of completeness, we show the form the boundary layer equations assume on the stagnation line, once the Lees–Dorodnitsyn coordinate transformation is applied[16,19]:

Continuity:

$$\frac{\partial \tilde{V}}{\partial \hat{\eta}} + F = 0 \quad (7)$$

Species continuity:

$$\tilde{V} \frac{\partial y_i}{\partial \hat{\eta}} + \mathcal{K} \frac{\partial J_i}{\partial \hat{\eta}} = \dot{w}_i \quad (8)$$

Momentum:

$$\tilde{V} \frac{\partial F}{\partial \hat{\eta}} = \frac{1}{2}\left(\frac{\rho_e}{\rho} - F^2\right) + \frac{1}{2} \frac{\rho_e v_e}{\rho \beta_e^{t2}} \frac{\partial \beta_e^t}{\partial y} + \mathcal{K}^2 \frac{\partial}{\partial \hat{\eta}}\left(l_0 \frac{\partial F}{\partial \hat{\eta}}\right) \quad (9)$$

Energy:

$$\tilde{V} \frac{\partial g}{\partial \hat{\eta}} = \mathcal{K}^2 \frac{\partial}{\partial \hat{\eta}}\left(\frac{l_0}{Pr} \frac{\partial g}{\partial \hat{\eta}}\right) - \mathcal{K}^2 \frac{\partial}{\partial \hat{\eta}}\left(\frac{l_0}{Pr} \sum_{i=1}^{Ns} \frac{\partial y_i}{\partial \hat{\eta}} \frac{h_i}{h_e}\right) - \mathcal{K} \frac{\partial}{\partial \hat{\eta}}\left(\sum_{i=1}^{Ns} J_i \frac{h_i}{h_e}\right) \quad (10)$$

By comparison to standard stagnation-line boundary layer equations written in Lees–Dorodnitsyn variables[16,21] one can notice the presence of two additional terms: $\mathcal{K}$ and the second term of the RHS of the momentum equation. In the classical boundary layer theory the outer edge quantities are computed by extrapolating the external inviscid solution to the wall. In the ground facility, instead, a low-Mach-number, low-Reynolds-number jet impinges on the TPS material sample and it is therefore more appropriate to match the

boundary layer (which should be seen as a zoom of the stagnation region) and the external flow at the real boundary layer outer edge. The two extra terms are due to such a matching procedure; $\mathcal{K}$ accounts for the real boundary layer thickness and the second term on the RHS of the momentum equation accounts for the fact that the quantity $\partial u_e/\partial y$ (computed at the boundary layer outer edge) has to be included in the expression of the boundary layer pressure gradient before the Lees–Dorodnitsyn transformation is applied.[16] The quantity $\mathcal{K}$ is constant along the stagnation line and it is computed during the numerical solution of the boundary layer equations.[16] The second term on the RHS of Eq. (9) is computed by means of data processing of ground experiments. The procedure combines experimental results with numerical computations of the flowfield inside the ground facility; interested readers are addressed to Refs. 8 and 9.

The second series of computations, for the real flight condition, are performed by means of a Navier–Stokes finite volume code for reacting flows, which was also developed by the first author.[16,22] The convective terms are discretized with the hybrid upwind splitting Riemann solver.[23] A total variation diminishing type reconstruction[24] is applied to achieve second-order accuracy; Van Albada's limiter is used in the present work. The transport terms are centrally discretized with second-order accuracy.

The two codes make use of the same set of physicochemical models, thus allowing a coherent and physically consistent comparison between the two series of computations. In Ref. 19 it is shown that the two codes provide results in excellent agreement when they are applied to the same problem.

Wind Tunnel and Flight Data Determination

The external flowfield conditions in the stagnation region of the TPS material sample are taken from data of existing experiments.[8,9] The first set of data, hereafter called case (a), has been obtained from the VKI Minitorch experiments, a small-scale plasma wind tunnel.[8] The second set of data, hereinafter called case (b), has been taken from experiments carried out in the VKI Plasmatron facility.[25] These two examples are chosen to illustrate the validity of the LHTS concept.

The following conditions are selected for case (a):

$$H_e^t = 9.8(\mathrm{MJ/kg}) \qquad p_e^t = 10161\,\mathrm{Pa} \qquad \beta_e^t = 11670\,\mathrm{s}^{-1} \quad (11)$$

(These have to be understood as conditions at the TPS boundary layer outer edge.) Under the assumption of local equilibrium, they correspond to a temperature $T_e^t = 4560$ K and to a chemical composition where molecular oxygen is almost fully dissociated and molecular nitrogen is just starting to dissociate.

Extrapolation of these wind tunnel conditions to the real flight ones, by the method previously described, gives

$$V_\infty^f = 4430\,(\mathrm{m/s}) \qquad M_\infty^f = 13.7 \qquad z_\infty^f = 55.78\,\mathrm{km}$$
$$p_\infty^f = 38\,\mathrm{Pa} \qquad T_\infty^f = 258.6\,\mathrm{K} \qquad R_\infty^f = 17.72\,\mathrm{cm} \quad (12)$$

where z_∞^f is the altitude, which has been determined from the U.S. 1976 Standard Atmosphere. The computed speed value is within the upper 10% of the space shuttle speed at the same altitude.[3] For simplicity the shape of the (re-)entry body has been taken to be a sphere with a radius equal to R_∞^f. The predicted body nose radius is too small compared with that of existing or planned (re-)entry vehicles.

A more realistic (re-)entry vehicle nose radius is obtained for case (b), to which the following conditions apply:

$$H_e^t = 22.8(\mathrm{MJ/kg}) \qquad p_e^t = 12525\,\mathrm{Pa} \qquad \beta_e^t = 1502\,\mathrm{s}^{-1} \quad (13)$$

Under the assumption of local equilibrium, the boundary layer outer edge temperature is $T_e^t = 6085$ K, molecular oxygen is fully dissociated, and nearly 40% of molecular nitrogen is dissociated. The real flight conditions are

$$V_\infty^f = 6755\,(\mathrm{m/s}) \qquad M_\infty^f = 21.5 \qquad z_\infty^f = 60.96\,\mathrm{km}$$
$$p_\infty^f = 19\,\mathrm{Pa} \qquad T_\infty^f = 244.4\,\mathrm{K} \qquad R_\infty^f = 1.79\,\mathrm{m} \quad (14)$$

The air mixture considered for both cases is a five-component mixture: molecular oxygen, O_2, molecular nitrogen, N_2, nitric oxide, NO, atomic oxygen, O, and atomic nitrogen, N. Because of the relatively low temperature there is no need to take into account ionized species.

Numerical Results and Flight Extrapolation

To assess local heat transfer two series of computations have been performed for each test case. A first series of computations is performed along the stagnation line of the TPS material sample by the boundary layer method. A second series of computations, for the real flight condition, has been performed by means of the Navier–Stokes finite-volume technique.

Six different levels of wall catalytic activity have been taken into account. The wall reaction set is given by $N + N \rightarrow N_2$ and $O + O \rightarrow O_2$; i.e., we take into account recombination of atomic nitrogen and of atomic oxygen at the wall, and we also assume that the wall has no effect on nitric oxide, NO. For simplicity, a single value of the catalytic recombination probability γ has been taken for the two reactions. The six different computations correspond to the following values of γ:

$$\gamma = \{0;\ 10^{-4};\ 10^{-3};\ 10^{-2};\ 10^{-1};\ 1\}$$

The wall temperature T_w has been taken as uniformly equal to 1000 K both on the TPS sample and on the equivalent (re-)entry geometry.

The boundary layer computations have been performed only at the stagnation point: 100 points in the direction across the boundary layer have been taken for both case (a) and case (b). Doubling the number of grid points affects the computed heat flux by less than 0.5%. The Navier–Stokes computations have been performed on the front part of the sphere and only half of it has been considered, because of the symmetry with respect to the stagnation line. The grid has 3600 cells for case (a) and 5680 for case (b), and it is suitably refined in the boundary layer and in the proximity of the bow shock in order to improve the computational accuracy. We also checked the accuracy of the computation: doubling the number of cells changes the computed heat flux by less than 2%, for both case (a) and (b).

We discuss now the results for case (a). In Fig. 1, the heat flux computed for the different values of the catalytic recombination probability γ is shown (the heat flux value for $\gamma = 0$ is not shown because of the logarithmic scale, but it is practically equal to that for $\gamma = 10^{-4}$). The difference in heat flux between the Navier–Stokes and boundary layer computations goes from 3% for the case of a noncatalytic wall to 37% for the case of a fully catalytic wall. Although the difference in heat flux for a fully catalytic wall is probably too high, the difference in the case of a noncatalytic or low-catalytic ($\gamma < 10^{-3}$) wall (which is the case of interest for aerospace applications) is below 6%, i.e., in range of experimental uncertainty.[7]

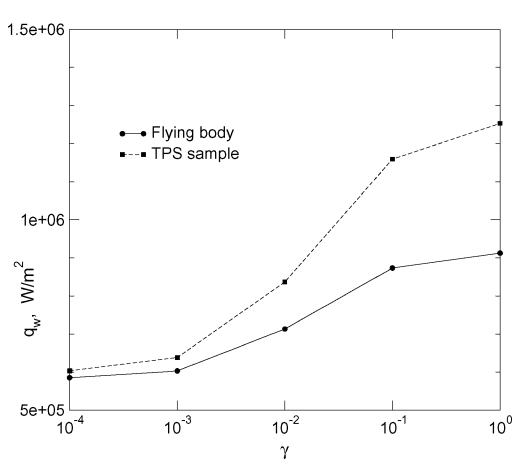

Fig. 1 Case (a): stagnation point heat flux for different catalyticity levels.

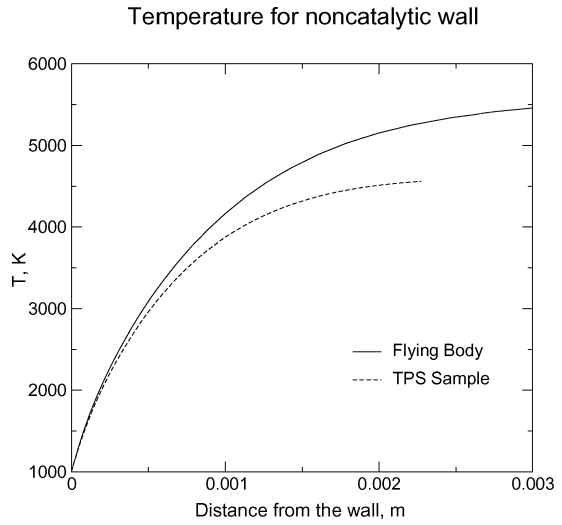

Fig. 2 Case (a): temperature profile for noncatalytic wall.

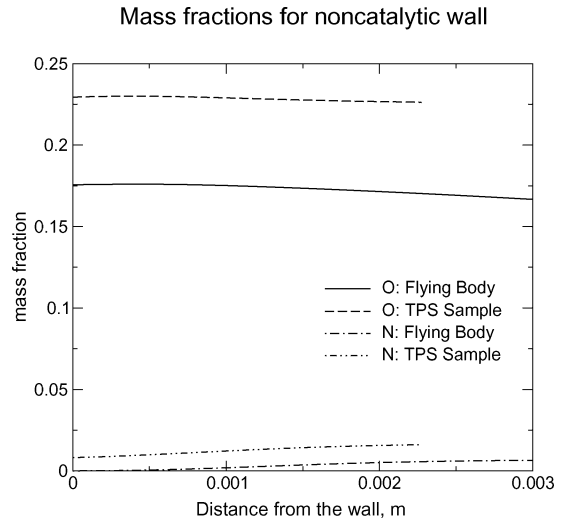

Fig. 3 Case (a): O and N mass fractions for noncatalytic wall.

The reason for the good agreement between the two computations in the case of a low- or noncatalytic wall can be seen in Figs. 2 and 3. The temperature profiles are similar in the portion of the boundary layer with $y < 0.001$m and the respective slopes at the wall are almost identical (see Fig. 2). This leads to good agreement on the conductive part $(-\lambda \nabla T)$ of the heat flux between the two configurations. Looking at Fig. 3 one can notice that the boundary layer is practically frozen in both computations; the diffusive part of the heat flux

$$\left(\sum_{i=1}^{N_s} h_i \boldsymbol{J}_i \right)$$

is thus negligible in the two cases (and zero for the noncatalytic case). The atomic oxygen mass fraction is higher for the TPS sample than for the flying body, but the two profiles have an almost identical shape, differing only by a constant shift. The same observations are valid for atomic nitrogen. This similar behavior is not surprising, because Eq. (6) implies the equality of the first Damköhler number in the stagnation regions of both the TPS sample and the real flight body. The inverse of the velocity gradient is in effect a time scale of the flow and it is the same for both configurations. The outer edge temperature and pressure being the same, the chemical characteristic time is also the same and, therefore, the first Damköhler number. Another parameter that has to be correctly reproduced is the second Damköhler number, which characterizes the heterogeneous chemistry–diffusion coupling and therefore the interaction between the TPS material and the gas. The second Damköhler number is defined as $Da_2 = k_S l^2 / D$, where k_s is the inverse of a characteristic time of the wall heterogeneous reactions, D a diffusion coefficient, and l a characteristic length over which diffusion takes place (such as, for example, the boundary layer thickness). The surface material is the same and, therefore, k_s is the same too; in addition, because pressure, temperature, and chemical composition are similar, D is also the same. Looking at Figs. 2 and 3 we notice that the boundary layer thickness l is fairly close in the two configurations: in effect, stagnation point boundary layer thickness is a function of the square root of the inverse of velocity gradient.[20] Therefore we deduce that the second Damköhler number is also acceptably duplicated in the ground facility.

A good reproduction of the behavior of atomic species, especially oxygen, in the ground facility is important to ensure that phenomena such as aging and oxidation of the TPS material are correctly simulated. In the specific case, the overestimation of atomic oxygen mass fraction for the TPS sample in the test configuration gives a certain safety margin.

The fact that temperature is higher and atomic species mass fractions are lower at the boundary layer edge in the flying body case than in the TPS sample case means that in the former configuration there is still a certain degree of nonequilibrium in the shock layer, thus violating one of the assumptions on which the LHTS concept is based. However, the influence of the violation is negligible (at least for heat flux determination) in the case of a low catalytic wall.

In Fig. 4 the temperature profiles for a fully catalytic wall ($\gamma = 1$) are shown. The agreement is even better than before and the conductive part of the heat flux is within 2% in the two configurations. Therefore, the difference in total heat flux (see Fig. 1) is due only to the diffusive part. Looking at Fig. 5, we notice that atomic species are recombining at the wall because it is fully catalytic. The chemical composition in the boundary layer is dominated in both cases by the wall reactions $O + O \rightarrow O_2$ and $N + N \rightarrow N_2$. Molecular oxygen and nitrogen created at the wall diffuse toward the interior of the boundary layer, completely changing the picture with respect to the noncatalytic case. We further notice that not only atomic oxygen mass fraction is higher for the TPS sample, but also its slope at the wall. This implies that the diffusive heat flux is higher in the TPS sample case than in the flying body one, thus explaining the observed differences in total heat flux (the contribution of atomic nitrogen recombination to the heat flux is negligible).

Results for case (b) are discussed now. In Fig. 6 the stagnation point heat flux, computed for several values of catalytic recombination probability γ, is shown. (As in case (a) the heat flux value for $\gamma = 0$ is not shown because of the logarithmic scale, but it is practically equal to the one for $\gamma = 10^{-4}$). Computed heat flux difference between Navier–Stokes and boundary layer goes from 2% for the

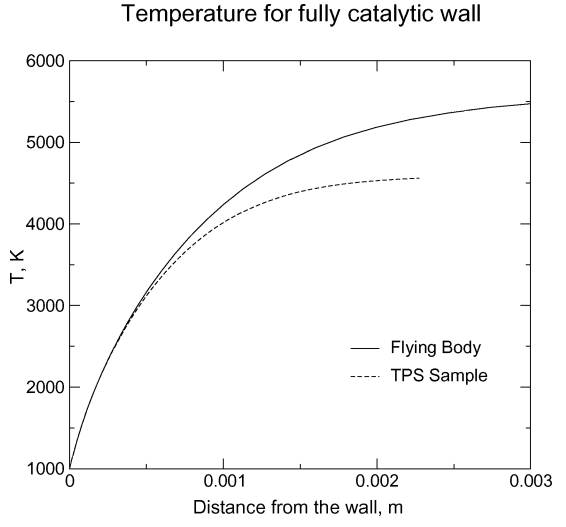

Fig. 4 Case (a): temperature profile for fully catalytic wall.

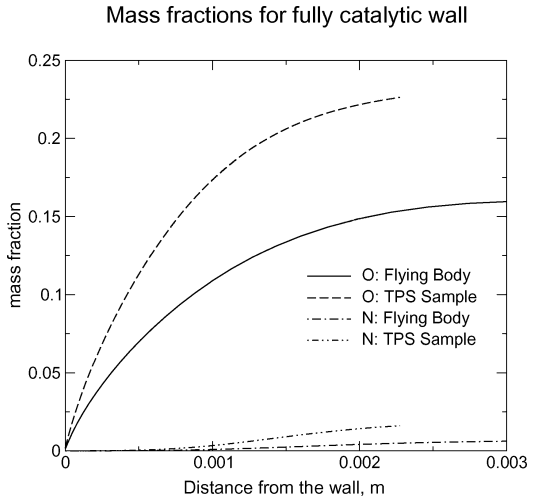

Fig. 5 Case (a): O and N mass fractions for fully catalytic wall.

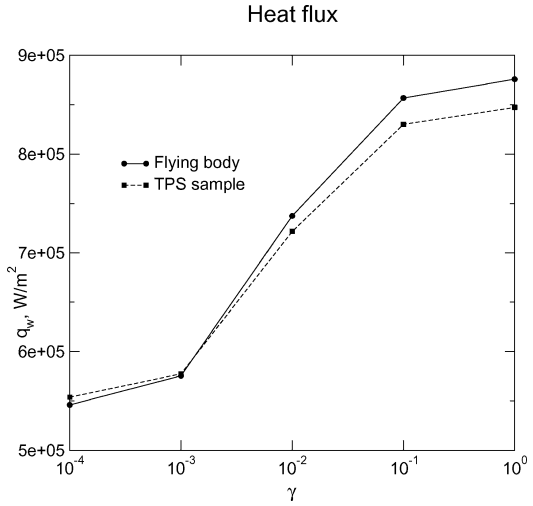

Fig. 6 Case (b): stagnation point heat flux for different catalyticity levels.

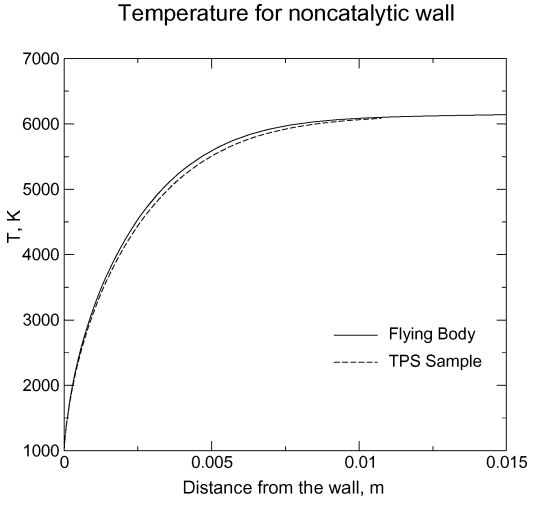

Fig. 7 Case (b): temperature profile for noncatalytic wall.

noncatalytic wall to 3% for the fully catalytic wall. We notice also that for the noncatalytic wall heat flux is higher for boundary layer computations, whereas for the fully catalytic wall heat flux is higher for Navier–Stokes computations.

In Fig. 7 temperature profiles for the noncatalytic wall are shown; the agreement is excellent, in particular close to the wall.

In Fig. 8, atomic species profiles for the noncatalytic wall are shown. Oxygen is fully dissociated at the boundary layer outer edge

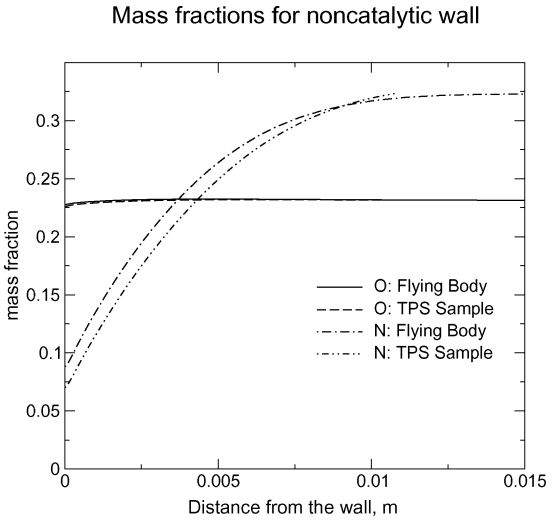

Fig. 8 Case (b): O and N mass fractions for the noncatalytic wall.

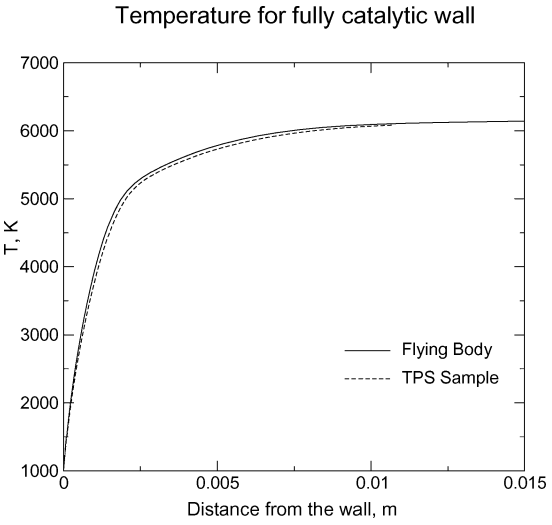

Fig. 9 Case (b): temperature profile for fully catalytic wall.

and remains fully dissociated all along the boundary layer; agreement between ground and flight profiles is excellent. Nitrogen is partially dissociated at the boundary layer edge. Agreement between TPS sample and flying body profiles is good, suggesting that the same physicochemical phenomena are happening in the two boundary layers. Compared with case (a) we notice a much improved agreement in atomic species profiles. The main reason is the close matching of boundary layer outer edge chemical composition between ground and flight. Chemistry is assumed to be in equilibrium at the TPS boundary layer outer edge and for case (b) is close to equilibrium for flight too. The main reason is that velocity gradient, which is the inverse of the typical flow time in the stagnation region, is now six times smaller than in case (a). We would also like to point out that, as in case (a), boundary layer thickness and first and second Damköhler numbers are well matched for TPS sample and flying body.

In Fig. 9 the temperature profiles for a fully catalytic wall are shown. The two temperature profiles are again very close to each other. One can notice that, at the same distance from the wall, temperature is higher for the fully catalytic wall than for the noncatalytic one.

Atomic species profiles are shown in Fig. 10. The atomic oxygen profile is strongly affected by wall catalytic recombination, because oxygen molecules created at the wall diffuse toward the interior of the boundary layer. Atomic nitrogen appreciably recombines in the bulk of the boundary layer and its slope at the wall is quite shallow, although the wall is fully catalytic. Both phenomena, wall-dominated recombination for O and gas-phase-dominated

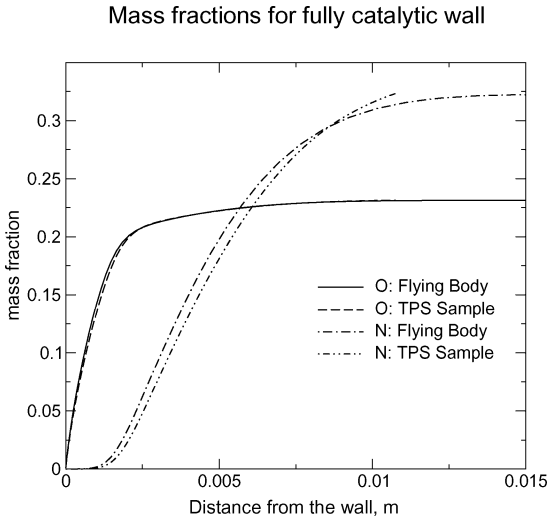

Fig. 10 Case (b): O and N mass fractions for fully catalytic wall.

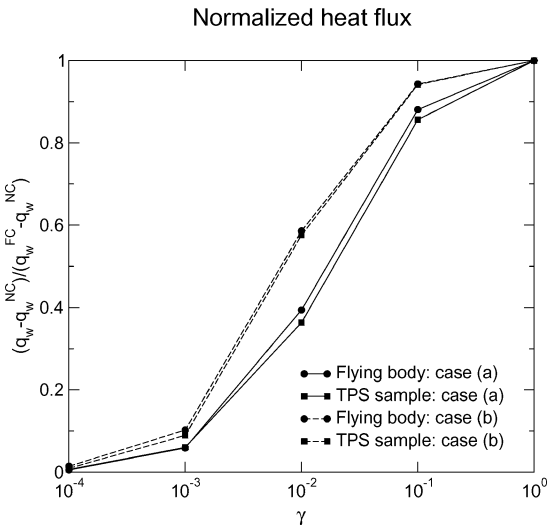

Fig. 11 Stagnation point normalized heat flux for different catalycity levels.

recombination for N, are reproduced with good agreement between TPS sample and flying body. The slope of the atomic species profile at the wall is modestly larger in the real body boundary layer, explaining the slightly higher flight heat flux.

From the previous discussion one could conclude that the local heat transfer simulation concept has only a limited range of validity, i.e., when the conditions at the boundary layer outer edge are close to local equilibrium. However, both curves in Fig. 1 and in Fig. 6 are similar and show a strong dependence of the heat flux from wall catalyticity in the interval 10^{-3}–10^{-1}; this suggests that the same physicochemical trends are reproduced in the ground facility and in flight. In addition, by looking at Fig. 11, we notice that the normalized heat flux

$$Q = \frac{q_w - q_w^{\mathrm{NC}}}{q_w^{\mathrm{FC}} - q_w^{\mathrm{NC}}} \tag{15}$$

is very similar for ground and flight in both cases (a) and (b). The excellent agreement between normalized heat fluxes is mainly due to the equality of Damköhler numbers for TPS sample and flying body. The flight heat flux for an arbitrary value of wall catalyticity could therefore be deduced by means of the formula

$$q_w^f = Q^t \cdot \left(q_w^{f,\mathrm{FC}} - q_w^{f,\mathrm{NC}}\right) + q_w^{f,\mathrm{NC}} \tag{16}$$

where Q^t is computed by means of Eq. (15) with the heat flux values obtained for the TPS sample; these values can also be experimentally measured ones. Equation (16) is very accurate. Consider, for example, the heat flux value for case (a) with $\gamma = 10^{-1}$: the TPS sample computation overpredicts the heat flux by 22% with respect to the real flight one. If, on the other hand, Eq. (16) is used, the heat flux is underpredicted only by 1%, a really dramatic improvement.

The normalized heat fluxes (Fig. 11) could be interpreted as the effect of boundary layer chemical activity on the heat transfer. Because the heat flux is always increasing with the wall catalyticity, the curves will be strictly monotonic. However, a curve standing in the lower part of the graph indicates lower gas chemical activity, whereas a curve lying in the upper part reveals higher chemical activity inside the boundary layer. In effect, in the limit case of chemical equilibrium, the heat flux is the same for every possible value of wall catalyticity[12] and the normalized heat flux curve collapses into a straight line corresponding to $Q = 1$. The relative positions of the curves for cases (a) and (b) could therefore be interpreted based on these considerations. Case (a), for instance, denotes a situation where the gas phase chemical activity is lower. This fact is due to the much higher velocity gradient for this case, which promotes a frozen flow at the stagnation region by imposing a lower Damköhler number. This characteristic can be noticed in Fig. 11: the curve for case (a) appears below the curve for case (b). In addit., inspection of Figs. 3 and 8 clearly points out that chemical activity in the boundary layer is higher in case (b) than in case (a).

Conclusions

The LHTS concept has been presented with its application to plasma wind tunnel experiments. Two examples allowed to illustrate the different aspects of the methodology and demonstrated that it correctly extrapolates ground test conditions to real flight ones. The equality of stagnation enthalpy, pressure and velocity gradient, plus the fact that the flow is near equilibrium in the stagnation region, are necessary for a correct reproduction of the flight thermochemical environment inside the ground facility. Deviations from the condition of local equilibrium in the stagnation region of the real body are mainly responsible for the discrepancies in heat flux determination between the ground facility and the flight. However, a normalized heat flux formulation can be used to account for these inconsistencies and to obtain an improved heat flux prediction.

Acknowledgments

We would like to thank A. F. Kolesnikov of IPM Moscow for his help and the fruitful discussions we have had.

References

[1]Prabhu, D.,"System Design Constraints—Trajectory Aerothermal Environments," *Critical Technologies for Hypersonic Vehicle Development*, edited by D. Gaitonde and D. Fletcher, NATO-RTO, Brussels, 2004.

[2]Kolodziej, P., "Strategy and Approach to TPS Design," *Critical Technologies for Hypersonic Vehicle Development*, edited by D. Gaitonde and D. Fletcher, NATO-RTO, Brussels, 2004.

[3]Anderson, J. D., *Hypersonic and High Temperature Gas Dynamics*, McGraw Hill, New York 1989.

[4]Neumann, R., "Experimental Methods for Hypersonics: Capabilities and Limitations," *The Second Joint Europe/US Short Course in Hypersonics*, US Air Force Academy Colorado Springs, CO 80840, Jan. 1989.

[5]Rose, P., and Stark, W., "Stagnation Point Heat Transfer Measurements in Dissociating Air," *Journal of the Aeronautical Sciences*, Vol. 25, No. 2, 1958, pp. 86–97.

[6]Stewart, D., Chen, Y., Bamford, D., and Romanovsky, A., "Predicting Material Surface Catalytic Efficiency Using Arc-jet Tests," AIAA Paper 95-2013, 1995.

[7]Kolesnikov, A. F., "Combined Measurements and Computations of High Enthalpy and Plasma Flows for Determination of TPM Surface Catalycity," *Measurement Techniques for High Temperature and Plasma Flows*, edited by J. M. Charbonnier and G. S. R. Sarma, NATO-RTO, Brussels, 1999.

[8]de la Llave Plata, M., "Analysis and Application of a Methodology for the Determination of TPS Materials Catalyticity," Diploma Project Report, 2000-4, von Karman Institute, Rhode-St-Genese, Belgium, June 2000.

[9]Degrez, G., Barbante, P. F., de la Llave Plata, M., Magin, T., and Chazot, O., "Determination of the Catalytic Properties of TPS Materials in the VKI ICP Facilities," ECCOMAS, Barcelona, Sept. 2001.

[10]Chazot, O., Paris, S., Collin, P., Bickel, M., and Ullman, T., "TPS Testing and Catalycity Determination in the VKI Plasmatron Facility," Association Aeronautique et Astronautique de France, Paris, March 2003.

[11]Kolesnikov, A. F., "The Concept of Local Simulation for Stagnation Point Heat Transfer in Hypersonic Flows: Applications and Validation," AIAA Paper 2000-2515, 2000.

[12]Fay, J. A., and Riddell, F. R., "Theory of Stagnation Point Heat Transfer in Dissociating Air," *Journal of the Aeronautical Sciences*, Vol. 25, No. 2, 1958, pp. 73–85.

[13]Goulard, R., "On Catalytic Recombination Rates in Hypersonic Stagnation Heat Transfer," *Jet Propulsion*, Vol. 28, No. 11, 1958, pp. 737–745.

[14]Lunev, V. V., *Hypersonic Aerodynamics*, Maschinostroenie, Moscow, 1975. (In Russian.)

[15]Bottin, B., and Vanden Abeele, D., Carbonaro, M., Degrez, G., and Sarma, G. S. R., "Thermodynamic and Transport Properties for Inductive Plasma Modeling," *Journal of Thermophysics and Heat Transfer*, Vol. 13, No. 3, 1999, pp. 343–350.

[16]Barbante, P. F., "Accurate and Efficient Modeling of High Temperature Nonequilibrium Air Flows," Ph.D. Thesis, Université Libre de Bruxelles-von Karman Institute, Brussels, Belgium, 2001.

[17]Sutton, K., and Gnoffo, P., "Multi-Component Diffusion with Application to Computational Aerothermodynamics," AIAA Paper 98-2575, 15–18 June 1998.

[18]Gupta, R. N., Yos, J. M., Thompson, R. A., and Lee, K. P., "A Review of Reaction Rates and Thermodynamic and Transport Properties for an 11-Species Air Model for Chemical and Thermal Nonequilibrium Calculations to 30000 K," RP 1232, NASA, Aug. 1990.

[19]Barbante, P. F., Degrez, G., and Sarma, G. S. R., "Computation of Nonequilibirum High-Temperature Axisymmetric Boundary-Layer Flows," *Journal of Thermophysics and Heat Transfer*, Vol. 16, No. 4, 2002, pp. 490–497.

[20]White, F. M., *Viscous Fluid Flows*, 2nd ed., Ch. 3, McGraw–Hill, New York, 1991.

[21]Fletcher, C. A. J., *Computational Techniques for Fluid Dynamics*, 2nd ed., Vol. 2, Ch. 15, Springer-Verlag, Heidelberg, 1991.

[22]Barbante, P. F., and Degrez, G., "An Efficient Euler/Navier–Stokes Solver for Reacting Flows," IMACS, Brussels, August 2000.

[23]Coquel, F., and Liou, M. S., "Hybrid Upwind Splitting Scheme by a Field by Field Decomposition," TM 106843, NASA, Jan. 1995.

[24]Hirsch, C., *Numerical Computation of Internal and External Flows*, Vol. 2, Wiley, Chichester, UK, 1990.

[25]Bottin, B., and Chazot, O., Carbonaro, M., Van Der Haegen, V., and Paris, S., "The VKI Plasmatron Characteristics and Performance," *Measurement Techniques for High Temperature and Plasma Flows*, edited by J. M. Charbonnier and G. S. R. Sarma, NATO-RTO, Brussels, 1999.